J Solid State Electrochem (2014) 18:399–409
DOI 10.1007/s10008-013-2232-y

ORIGINAL PAPER

Monitoring stabilizing procedures of archaeological iron using electrochemical impedance spectroscopy

Antonio Doménech-Carbó · Monserrat Lastras · Francisco Rodríguez · Emilio Cano · Juan Piquero-Cilla · Laura Osete-Cortina

Received: 28 May 2013 / Revised: 14 August 2013 / Accepted: 16 August 2013 / Published online: 29 August 2013

Abstract A methodology for monitoring washing procedures applied to stabilize archaeological iron is described. It is based on the combination of voltammetry of microparticles (VMP) with electrochemical impedance spectroscopy (EIS). A semi-empirical approach is used where the impedances at low and high frequencies were related with the fraction areas of passive and corrosion layers generated during the stabilizing treatment, the thickness, and the porosity of the corrosion layer. The variation of such parameters with the time of washing was determined from EIS data for four types of desalination procedures using concentrated NaOH and/or Na_2SO_3 aqueous solutions on archaeological iron artifacts. After 2 months of treatment, EIS data indicate that an essentially identical "stable" state was attained in all cases, as confirmed by the formation of a passive magnetite layer identified in VMP measurements while the rate of variation of corroded surface and porosity at short washing times varied significantly from one stabilization procedure to another.

Keywords Archaeological iron · Desalination methods · Electrochemical impedance spectroscopy · Voltammetry of microparticles · Conservation–restoration

A. Doménech-Carbó (✉) · J. Piquero-Cilla
Departament de Química Analítica, Facultat de Química, Universitat de València, Dr. Moliner 50, 46100 Burjassot, Valencia, Spain
e-mail: antonio.domenech@uv.es

M. Lastras · F. Rodríguez · L. Osete-Cortina
Institut de Restauració del Patrimoni, Universitat Politècnica de València, Camí de Vera 14, 46022 València, Spain

E. Cano
Centro Nacional de Investigaciones Metalúrgicas (CENIM), Consejo Superior de Investigaciones Científicas (CSIC), Avda. Gregorio del Amo 8, 28040 Madrid, Spain

Introduction

The corrosion of archaeological iron artifacts results in a mineralization of the surface which becomes hidden by corrosion products. Subsequently, the metal core continues to corrode what provokes flaking of the mineral crust, until the metal core is completely oxidized. Finally, the objects lose entirely their shape and become unsuitable for archaeological studies [1]. Stabilization of iron archaeological pieces is an essential prerequisite for their study and conservation [2, 3]. In short, the purpose of desalination procedures is stopping the progress of corrosion via formation of a passive layer, typically composed by magnetite, and removing chloride ions strongly favoring the advance of the corrosion process [4, 5]. Although the alkaline sulfite method, originally due to North and Pearson [6], theoretically accomplishes such requirements [7, 8], a variety of desalination methods consisting of washing the iron artifact with concentrated (0.1–1 M) NaOH, Na_2SO_3, and NaOH+ Na_2SO_3 aqueous solutions have been proposed [9, 10]. Proposed modifications involve the use of deoxygenated solutions [11], vacuum [12], alkylammonium solutions in nonaqueous solvents [13, 14], ultrasonication [15], and subcritical alkaline solutions [16, 17]. Electrochemical treatments have been also reported [18–21].

In this context, monitoring chloride concentration in desalination baths has received attention because of the importance of the washing process. The kinetics of chloride release by archaeological iron has been recently modeled by Selwyn et al. [22]. However, working with archaeological objects makes particularly difficult the application of analytical techniques for assessing the state of the artifact during the stabilizing treatment, in particular for estimating chloride concentration remaining in the objects, composition of the surface regions, etc. [23].

In previous contributions, we have reported the possibility of exploiting the voltammetry of microparticles (VMP) for

mapping corrosion products on archaeological pieces [24]. VMP is an electrochemical technique developed by Scholz et al. [25–27] whose application in the fields of archaeometry, conservation, and restoration has been recently reviewed [28–31], in particular with regard to tracing, authentication, and dating archaeological metal [32, 33]. Here, we report a combined application of VMP with electrochemical impedance spectroscopy (EIS) for comparing stabilization procedures applied to archaeological iron. EIS has been extensively used for monitoring metal corrosion [34–47], in particular, as recently reviewed by Cano et al. [48], for evaluating protective coatings on archaeological metal. Recently, Grassini et al. [49] have used EIS for an in situ corrosion study of Middle Ages wrought iron bar chains in the Amiens Cathedral while Hernandez-Escampa et al. [50] have used this technique for an assessment of the restoration and conservation of a heavily corroded archaeological iron artifact. Such studies can be viewed within the context of modeling of the general corrosion damage to metals and alloys and the acquisition of values for various model parameters. These include the high field model [51] and, more recently, the point defect model developed by Macdonald et al. [52–54]. This model provides a good account of the growth of the passive film on iron, and the extracted model parameters can be used to predict the corrosion evolution of the sample as a function of time, as recently reviewed [55]. The EIS technique, usually applied to metal probes, has been applied here to real archaeological artifacts using a special electrochemical cell. The irregular surface and electrical connection of such archaeological objects produce specific difficulties minimized here by using non-degasified aqueous $NaClO_4$ electrolyte and performing EIS experiments at the potential of the reduction of dissolved oxygen.

The proposed methodology is based on monitoring the composition of the surface layers of the iron artifact submitted to washing treatment and obtaining information on the variation of texture, porosity, and mineralization of archaeological objects during the desalination/stabilization process. Four classical desalination baths, namely 0.10 M NaOH, deoxygenated NaOH 0.10 M, both at room temperature, and 0.05 M Na_2SO_3+0.05 M NaOH at room temperature and at 50 °C, were compared.

Experimental

Electrochemical instrumentation and procedures

Voltammetry of microparticles experiments were performed at sample-modified paraffin-impregnated graphite electrodes (PIGEs; geometrical area 0.785 cm^2) immersed into 0.10 M HCl degasified by bubbling Ar, using a CH I660 potentiostat. PIGEs were prepared by impregnated pyrolitic graphite bars in vacuo as described in literature [25–27]. A standard three-electrode arrangement was used with a platinum auxiliary electrode and a Ag/AgCl (3 M NaCl) reference electrode. Few nanograms of sample were abrasively transferred to the surface of the PIGE as already described [28].

EIS measurements were performed, using the aforementioned instrument, in the 0.01- to 100,000-Hz frequency range with amplitude of 10 mV at different potentials between +1.00 and −1.00 V upon partial immersion of the archaeological piece in non-degasified 0.10 M $NaClO_4$ (Merck) aqueous solution. A home-made cell consisting of a 200-mL vessel coupled with a Teflon cover with three circular windows and auxiliary supporting bars as schematized in Fig. 1 was used. The archaeological pieces were suspended from an insulating tong and immersed to a certain depth and served as a working electrode upon connection to a conventional crocodile clamp. For each piece, experiments were performed for three different immersion depths and varying the position of the clamp. Three repeated experiments were performed for each one of these (depth plus clamp position) configurations.

Archaeological samples and desalination procedures

Archaeological iron samples consisted of fragments from pieces providing from the ancient Alcantarins convent in Ontinyent, dated in the nineteenth–twentieth AD centuries and the Torre la Sal archeological site in Oropesa, corresponding to the Iberian-Roman period (IVth BC), both studied since 2004. Original objects were discovered under burial conditions in calcareous soils and conserved metal cores (determined by x-radiography). All samples were fragments separated from the artifacts during their extraction and storage conserved in the repository of the Institut de Restauració del

Fig. 1 Photographic image of the EIS cell with an iron nail from the Alcantarins convent (Ontinyent, Valencian Community, Spain) serving as a working electrode

Patrimoni, Universitat Politècnica de València. The fragments were desalinated at room temperature using recently recommended washing solutions [23]: (a) 0.10 M NaOH, (b) nitrogen-deoxygenated 0.10 M NaOH, and (c) 0.05 M Na_2SO_3+0.05 M NaOH. A fourth desalination procedure was performed (d) by means of 0.05 M Na_2SO_3+0.05 M NaOH maintained at 50 °C in a thermostated bath. Aliquots of 5 mL were periodically extracted in order to determine the concentration of chloride. Then, the artifact was separated from the washing bath, rinsed repeatedly with bi-distilled water, and dried with paper. Then, the piece was used for EIS experiments and subsequently rinsed with water, dried, and immersed again in the desalination bath.

Results and discussion

Preliminary considerations

Monitoring the progress of desalination processes on archaeological iron artifacts involves some particular requirements: Experimental techniques should not be interfering with the desalination process itself and should not be invasive, i.e., their application should not alter the physical and chemical properties of the object. The use of genuine archaeological artifacts, with irregular, often highly corroded, surfaces, makes difficult their analysis by means of open-circuit potential (OCP) and potentiodynamic polarization curve (PPC) techniques where more or less significant Faradaic processes could occur.

In this context, EIS appears as a potentially usable technique for monitoring, ultimately, the time variation of properties such as porosity or effective surface area during the desalination process, but there is a fundamental aspect to be considered. Strictly, impedance is only defined for a stationary system fulfilling the constraints of the linear systems theory (LST). The measured system should be time invariant during the time of acquisition of the EIS data. The Kramers–Kronig (K–K) transforms can be applied to determine whether the impedance data are influenced by time-dependent phenomena and have been used the self-consistency of EIS data. Accordingly, even though that the time scale of the EIS experiments (tens of minutes) is much shorter than the desalination treatments (several weeks), it has to be tested if the "impedance" measured under our experimental conditions correctly transforms according to the K–K transforms [37, 56]. Pertinent data will be provided in the next section.

EIS cell design and performance

Figure 1 shows a photographic image of the electrochemical cell fabricated for testing archaeological iron pieces 1–10 cm sized. Under these conditions, well-defined PPC and OCP measurements were performed, but relatively large variability was obtained for different pieces. Additionally, experiments were sensitive to the area of the immersed region and the position of the clamp contact. Typical curves can be seen in Fig. 2, where potentiodynamic polarization curves for a chain link and a nail from the Alcantarins convent in contact with 0.15 M $NaClO_4$ are shown. Both curves show almost symmetrical Tafel regions around the corrosion potentials at +0.25 and +0.57 V vs. Ag/AgCl, respectively, and were followed by a passive region at positive potentials. Successive measurements on the same piece, however, produced significant shifts in both the OCP and PPC records. These features suggest that, under our experimental conditions, such techniques are not easily usable for monitoring desalination processes on archaeological artifacts. For this purpose, EIS experiments, where non-important Faradaic processes occur, were performed.

Preliminary experiments showed that EIS data were sensitive to the area of the immersed region, the position of the clamp contact, and the applied potential. In the low-frequency range. After testing EIS at potentials between +0.85 and −0.85 V vs. Ag/AgCl, the potential of −0.65 V vs. Ag/AgCl was selected. At this potential and in neutral aqueous solutions, there is no significant proton-assisted reductive dissolution of iron corrosion compounds [57, 58], while the reduction of dissolved oxygen, although kinetically constrained, can occur to any extent [59, 60], thus acting as a redox probe for EIS measurements.

Figure 3 compares the experimental transfer function for a chain link from the Alcantarins convent (Ontinyent, Valencian Community, Spain) and the transfer function calculated using K–K relations as described by Bastidas et al. [37]. An excellent agreement was obtained, thus denoting that, under our experimental conditions, the LST constraints are satisfied.

Typical impedance spectra recorded under such conditions are shown in Figs. 4 and 5. Bode plots of log(total impedance)

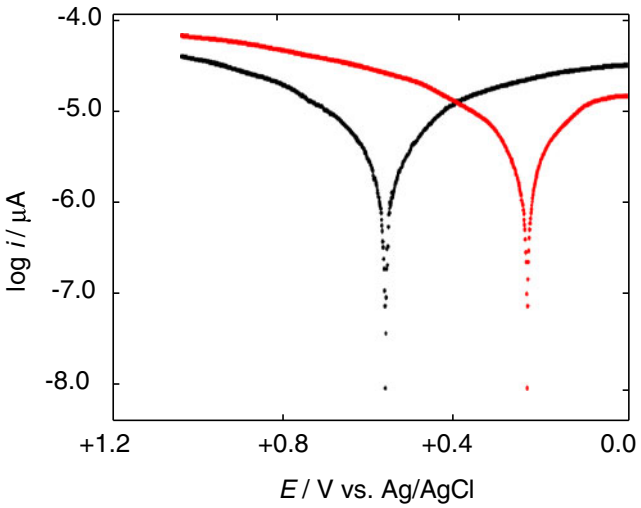

Fig. 2 Potentiodynamic polarization curves for a chain link (*black*) and a nail (*red*) in contact with 0.15 M $NaClO_4$. Potential scan rate 10 mV/s

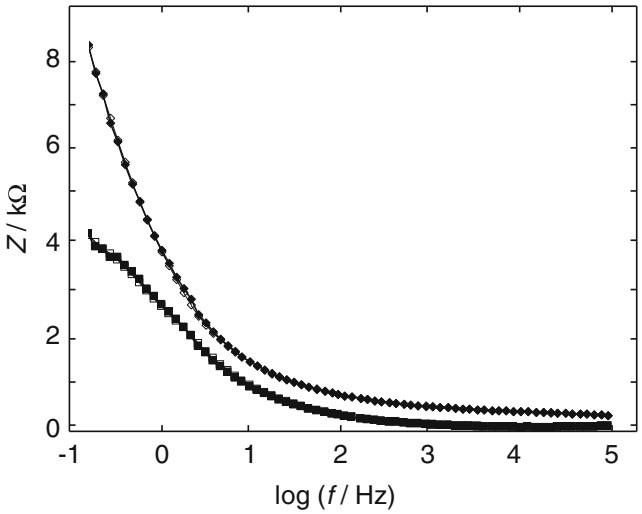

Fig. 3 Comparison of experimental transfer function for a chain link from the Alcantarins convent (Ontinyent, Valencian Community, Spain) immersed into air-saturated 0.15 M $NaClO_4$, recorded after 30 days of washing in 0.10 M NaOH, applied potential −0.65 V vs. Ag/AgCl, and transfer function calculated using K–K relations as described by Alves and Brett [38]. *Squares* real component, *rhombs* imaginary component, *solid figures* experimental data points, *empty figures* theoretical points

vs. log(frequency) (log$Z$ vs. log$f$) consist of typical s-shaped curves with log$Z$ monotonically decreasing on increasing log$f$ while Bode plots of phase angle vs. log(frequency) (φ vs. log$f$) fall in the capacitive region showing a maximum (in absolute value) at intermediate frequencies. Nyquist plots (see Fig. 5) consist of a capacity depressed semicircle with a distinctive 45 deg tail in the low-frequency region, attributable to the diffusion of species through the pores of the corrosion products [34, 44, 45] and/or protective coatings [35, 37, 39, 43]. In several cases, it appears a short "inverse" semicircle at high frequencies which can be attributed, at least partially, to inductances of the electrodes, the cables, or instrumental artifacts.

Under these conditions, EIS curves showed an excellent repeatability for measurements performed at a given immersion level and a given position of the connecting clamp (see Fig. 4). Upon varying the position of the connecting clamp and the depth, the impedance spectra, although retaining the general profile, varied significantly. Interestingly, however, there were regular variations between different EIS parameters for each one of the pieces, and those parameters varied systematically with the washing time during stabilizing treatments, as can be seen in Fig. 6. In this figure, the variation of $|Z|$ at a frequency of 10^{-1} Hz (Z_{-1} in the following) with $|Z|$ at a frequency of 10^{5} Hz (Z_5 in the following) for different archaeological pieces is shown. The use of such parameters was inspired in the approach described by Chen et al. [61] on modeling porous electrodes, based on the assumption that the real component of the impedance at the very high frequency ($Z_{\mathrm{real,f}\to\infty}$) corresponds to the ionic resistance of the electrolyte together with all the external resistances, while the limiting interfacial resistance at the very low frequency ($Z_{\mathrm{real,f}\to 0}$)

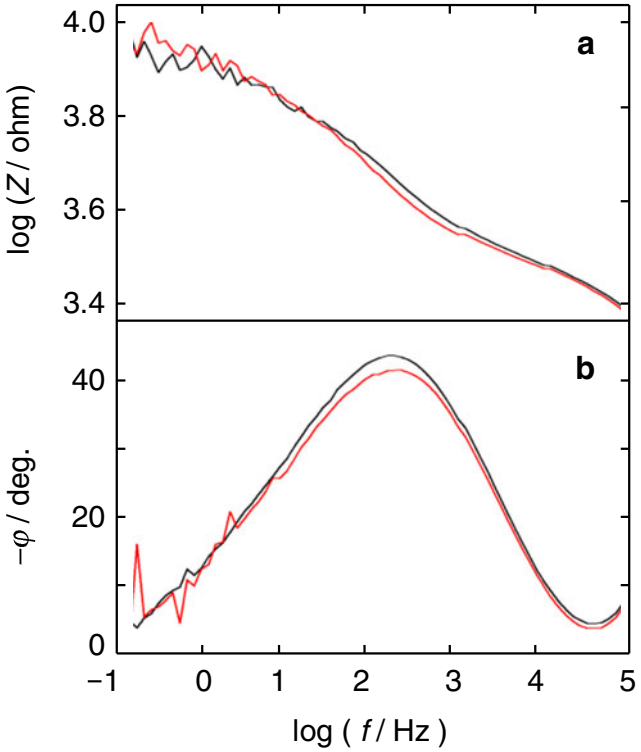

Fig. 4 Bode plots of *a* log$Z$ vs. log$f$ and *b* phase angle vs. log$f$ of EIS for a fragment from a roman hoe from Torre la Sal archaeological site (Oropesa, Valencian Community, Spain). *Black* and *red lines* correspond to replicate experiments performed in contact with air-saturated 0.15 M $NaClO_4$. Applied potential −0.65 V vs. Ag/AgCl

represents the sum of the ionic resistance contribution from the electrolyte and the electronic resistance contribution from the electrode. On first examination, the Z_5 and Z_{-1} values determined in our experiments can be taken as a reasonable approach representative of $Z_{\mathrm{real,f}\to\infty}$ and $Z_{\mathrm{real,f}\to 0}$, respectively.

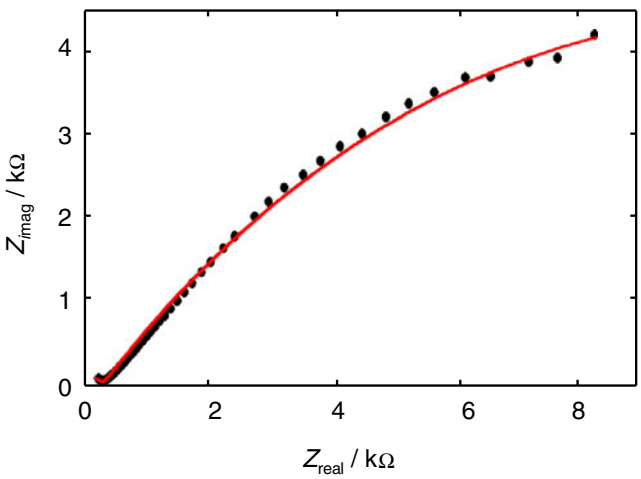

Fig. 5 Nyquist plots for EIS experiments at a chain link from the Alcantarins convent (Ontinyent, Valencian Community, Spain) immersed into air-saturated 0.15 M $NaClO_4$, recorded after 30 days of washing in 0.10 M NaOH. Experimental data points are superimposed to theoretical curve using parameters in the text

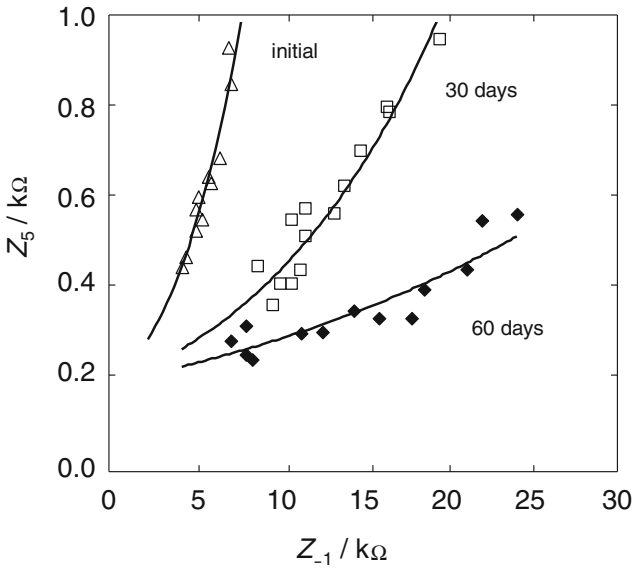

Fig. 6 Plots of Z_5 on Z_{-1} recorded from EIS data at different stages during the washing with 0.05 M Na_2SO_3+0.05 M NaOH of a nail from the Alcantarins convent. Data points correspond to EIS experiments varying the depth of immersion and the position of the connecting clamp of the archaeological piece in contact with air-saturated 0.15 M $NaClO_4$. Applied potential −0.65 V vs. Ag/AgCl

Experimental data on archaeological artifacts in this study provided apparently continuous variations of Z_5 on Z_{-1} varying with the washing time for each piece, as can be seen in Fig. 6. Similar regularities were obtained for other EIS parameters such as the maximum phase angle (in absolute value) and the frequency at which such maximum appears (vide infra). These features suggest that there is possibility of: (a) establishing an artifact-characteristic EIS response regardless of the immersion level and positioning of the clamp connection and (b) monitoring the evolution of the piece upon application of desalination procedures

EIS modeling

The above features can be examined on the light of existing knowledge on "electrochemical" iron corrosion. For iron corroded under burial conditions, chloride ions in the soil accumulate at anodic sites while layers of corrosion products build up the cathode preferentially, in principle, on magnetite areas due to the electrically conducting characteristics of this corrosion product. Iron oxidizes at anodic sites to Fe^{2+} ions, a process counterbalanced by a reduction reaction occurring at the cathodic sites, typically oxygen reduction and hydrogen evolution. After the initial corrosion process, solid Fe(II) hydroxide is formed and subsequently oxidizes to magnetite and Fe(III) hydroxide further yielding goethite. This process can passivate the iron as far as magnetite and goethite are thermodynamically stable [22]. Depending on the environmental conditions, however, the composition of the layer can change so that more or less hydrated Fe(III) hydroxyoxides mixed with extraneous material such as sand, clay, and soil minerals can be formed [2–4]. Chlorides will act as corrosion accelerators post-excavation [62]. As a result, the corrosion of archaeological iron pieces in atmospheric/soil environments can be described in terms of a local anode at the metal/atmosphere interface, where Fe metal is oxidized to Fe(II) forms, and a local cathode at the magnetite/atmosphere interface where atmospheric oxygen is reduced. As a result, the surface of the corroded artifact can be described as formed by an electron conducting core formed by a metal nucleus surrounded by a narrow layer of magnetite, covered by a discontinuous layer of more or less porous Fe(III) corrosion products [22].

For the purpose of EIS modeling, it is pertinent to consider that the impedance response of the system will be dependent on the electrical conductivity of the system, in turn conditioned by the remaining of a metallic nucleus or not, the structure, and the thickness, roughness, and porosity of the corrosion layers, as well as on the applied potential. As far as preliminary results provided the most stable EIS responses upon application of potentials negative enough to promote the electrochemical reduction of dissolved oxygen, EIS modeling was developed for this situation. Figure 7 shows a possible equivalent circuit for modeling the obtained EIS under these conditions where the piece acts as a cathode connected to the external anode completing the electrochemical cell. These conditions differ from those used by Grassini et al., operating at the OCP, where both anodic and cathodic processes were accounted [49]. Assuming that the electron conducting iron nucleus is entirely covered by a passive (presumably also electron conducting magnetite) layer, the circuit includes a

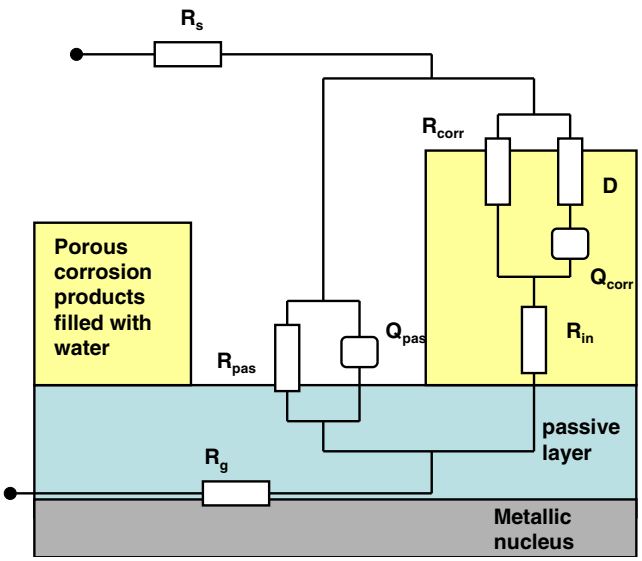

Fig. 7 Schematic representation of a fragment of corroded archaeological iron in contact with air-saturated aqueous electrolyte. Superimposed equivalent circuit used for modeling EIS measurements when a bias potential negative enough to promote reduction of dissolved oxygen is applied

solution resistance (R_s), a charge transfer resistance at the passive layer/electrolyte interface (R_{pas}), and interfacial capacitance of the passive layer/electrolyte contact, Q_{pas}, all these associated to the "ordinary" impedance spectrum of the conducting metal nucleus plus passive layer in contact with the electrolyte. To account for the corrosion layers, the charge transfer resistance at the corrosion layer/electrolyte interface, R_{corr}; the capacitance associated to the corrosion layer/electrolyte interface, C_{corr}; and one additional impedance associated to ion diffusion through the corrosion layer, D, can be included. To complete the circuit, account of the transport resistance in the metal nucleus and the conducting passive layer plus the artifact/connector contact, R_g, and the transport resistance of the corrosion layer and the corrosion layer nucleus (or passive layer) interface, R_{in}, can also be introduced, as in modeling of printing porous plates [63]. As a first refinement, capacitors can be replaced by constant phase elements in order to account for non-ideal capacitive behavior of the interfacial charge transfer mechanism associated with the nonuniform distribution of current. This non-ideality arises as a result of surface roughness, impurities, dislocations, or grain boundaries [38, 41, 42, 46, 47]. Figure 5 compares the experimental Nyquist plot with theoretical one from the model in Fig. 7 inserting R_s=10 Ω, R_g=50 Ω, R_{corr}= 150 kΩ, D=10 Ω, $Q_{corr}=9.1\times10^{-5}$ F, n_{corr}=0.55, R_{in}= 300 kΩ, R_{pas}=30 kΩ, $Q_{pas}=9.0\times10^{-8}$ F, and n_{pas}=0.76. As can be seen in Fig. 5, the above model provides a satisfactory fit with experimental data for archaeological metal pieces after washing. However, for original pieces (i.e., before submitting to desalination), there are major variability in the impedance response and, possibly, a more elaborated model including additional elements, eventually considering diffusion in restricted spaces [64, 65], would be required, in line with those proposed for describing layered mixtures of metal oxides created by anodic growth on metal surfaces [40, 66–68].

In order to favor the analysis of multiple artifacts, a semi-empirical treatment, based on the use of few EIS parameters, was carried out. First of all, variations of Z_5 on Z_{-1} in Fig. 6 can be attributed to the variations in the R_g and R_{in} terms associated to the different immersion level, positioning of the clamp, and local extent of the mineralization of the object. Then, for a given immersion level and clamp position, the difference $Z_{-1}-Z_5$ (= ΔZ_{tot}) can be taken, as a rough approximation, as representative of the combined ohmic resistance of the corrosion and passive layers, consistently with modeling of porous electrodes [61, 69]. The difference between the electrochemical polarization resistance including the charge- and mass-transfer resistances across the porous electrode and the solution resistance can be calculated as the difference between the real part of impedances at extremely low and high frequencies. Secondly, the above model produces two time constants. The first one corresponds to the electron transfer through the corrosion layer–electrolyte interface, and the characteristic frequency will be $\omega_1=1/R_{corr}C_{corr}$. The second is associated to the electron transfer through the passive layer-electrolyte interface, the characteristic frequency being $\omega_2=1/R_{pas}C_{pas}$. Then, the frequency at which the maximum (in absolute value) phase angle appears in Bode plots such as in Fig. 4 would be representative of the product $R_{corr}C_{corr}$.

VMP measurements

The variation in the composition of the corrosion and passivated layers of the studied samples was monitored by means of VMP measurements using the previously described "one-touch" sampling technique [24, 70, 71]. Figure 8 compares the SWV recorded on nanosamples extracted from a nail from the Alcantarins convent (Ontinyent, Valencian Community, Spain) before and after 30 days of its desalination in NaOH bath. Measurements were carried out using 0.10 M HCl as electrolyte, following previously reported procedure [24]. In the initial state, the corrosion layer contains mainly ochre-type materials displaying overlapping peaks between +0.20 and −0.05 V vs. Ag/AgCl, preceded by a chloride-based signal at +0.40 V vs. Ag/AgCl, and followed by a broad wave at −0.60 V vs. Ag/AgCl with a shoulder at ca. −0.20 V vs. Ag/AgCl. Upon prolonging the desalination watching, the above signals decrease progressively in height while a new, prominent peak at +0.10 V vs. Ag/AgCl appears. This peak can be attributed to the reduction of magnetite to FeO plus Fe^{2+} (aq) [72, 73].

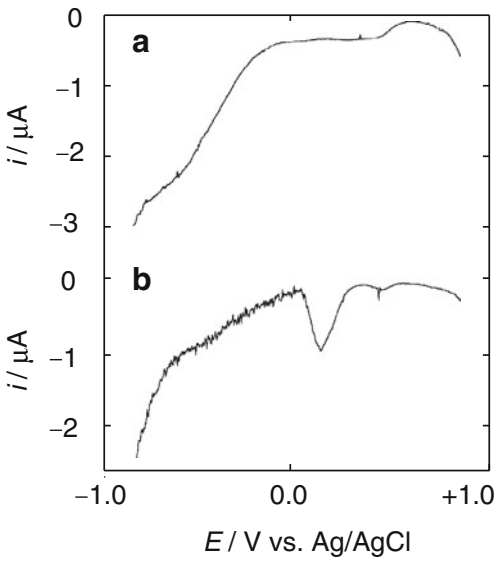

Fig. 8 SWV for "one-touch" extracted samples from a nail from the Alcantarins convent (Ontinyent, Valencian Community, Spain) submitted to watching in 0.10 M NaOH. *a* Initial state and sampling after *b* 30 days of desalination. Electrolyte 0.10 M HCl. Potential scan initiated at +0.65 V vs. Ag/AgCl in the negative direction; potential step increment 4 mV; square wave amplitude 25 mV; frequency 5 Hz

As can be seen in Fig. 9, corresponding to samples from clamp from the Alcantarins convent extracted by means of the "one-touch" procedure and submitted to 0.05 M Na_2SO_3+0.05 M NaOH, the chloride signal at +0.40 V vs. Ag/AgCl is retained whereas ochre peaks in the +0.20 to −0.20 V vs. Ag/AgCl potential region are removed and substituted by the magnetite peak at +0.10 V vs. Ag/AgCl. These results suggest that the advance of the desalination process can in principle be monitored by determining the growth of the magnetite peak at + 0.10 V vs. Ag/AgCl relative to the ochre signals. The main drawback for this purpose is that, in most archaeological pieces, the surface of the object presents irregularities and the composition becomes non-homogeneous, particularly at relatively short times during the stabilization of the piece. The use of VMP, however, permits to confirm unambiguously, given the high specificity of the magnetite signal [24], the formation of a stable, passive layer.

Monitoring desalination processes

Figure 5 permits to compare the theoretical and experimental Nyquist plots for a chain link immersed into 0.15 M $NaClO_4$, recorded after 30 days of desalination washing with NaOH 0.10 M. The Nyquist profile was qualitatively the same at all washing times, approaching the features described in the precedent section but on increasing the time of washing, the amplitude of the semicircular capacitive loop increased on prolonging the washing time. Similar features were observed for all other three desalination treatments. Consistently with the proposed modeling, the limiting value of Z_5 extrapolated for Z_{-1} tending to zero, theoretically equaling the R_s term, is the same for all washing times, as can be seen in Fig. 6.

The most remarkable changes in the EIS response were observed in Bode plots of the phase angle vs. log (frequency). As can be seen in Fig. 10, corresponding to a chain link from the Alcantarins site washed with 0.05 M Na_2SO_3+0.05 M NaOH, the (main) maximum in the phase angle is considerably shifted to higher frequencies on prolonging the duration of the desalination treatment, while the value of that angle increases slightly, as can be seen in Fig. 11 for replicate experiments on an archaeological chain link submitted to washing with 0.05 M Na_2SO_3+0.05 M NaOH and 0.10 M NaOH. Remarkably, the values of f_{max} are clearly insensitive to changes in the immersion level and the positioning of the connecting clamp and vary slightly from one artifact to another. These features can be attributed to the variations in the thickness, cohesion, degree of mineralization, and porosity of the corrosion layers resulting in a decrease of the charge transfer resistance and the double layer capacitance in the corrosion layer/electrolyte interface.

To rationalize time-dependent EIS parameters, we introduce the time-dependent fraction area of metallic nucleus, passive layer generated during the stabilizing treatment and corrosion layers (θ_{Fe}, θ_{pas}, θ_{corr}, respectively) in contact with the electrolyte solution, as described by Lee and Pyun to study corrosion resistance of surface-coated galvanized steel [68]. Under the simplifying assumptions introduced above, the difference between the limiting values of total impedance by surface area unit at low and high frequencies for an iron piece after a washing time t can be expressed as:

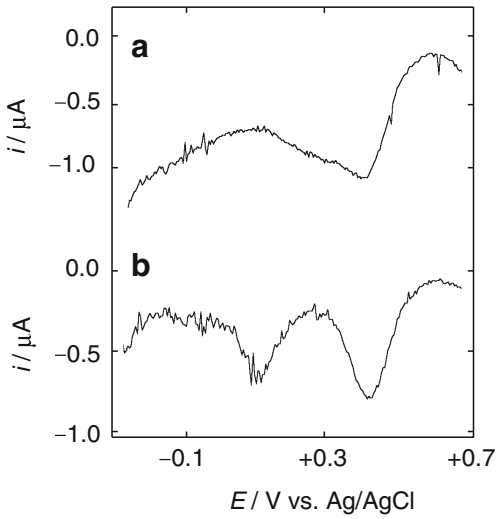

Fig. 9 Detail of SWV for "one-touch" extracted samples from a clamp from the Alcantarins convent (Ontinyent, Valencian Community, Spain) submitted to watching 0.05 M Na_2SO_3+0.05 M NaOH. a Initial state and after *b* 30 days of desalination. Electrolyte 0.10 M HCl. Potential scan initiated at +0.65 V vs. Ag/AgCl in the negative direction; potential step increment 4 mV; square wave amplitude 25 mV; frequency 5 Hz

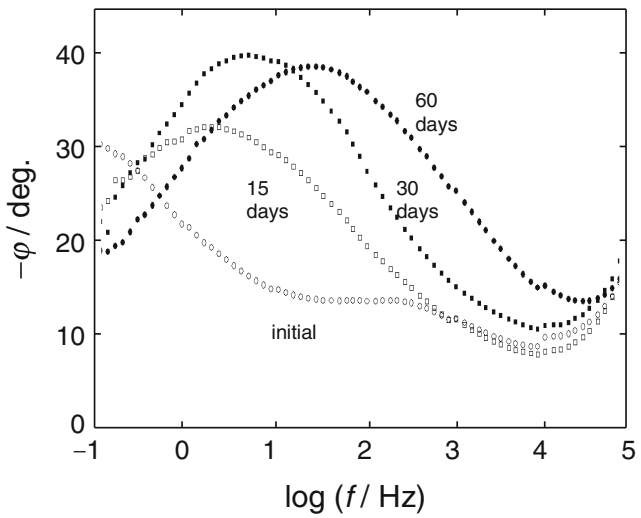

Fig. 10 Bode plots for EIS experiments at a chain link from the Alcantarins convent immersed into 0.15 M $NaClO_4$, recorded during different stages of its treatment with 0.05 M Na_2SO_3+0.05 M

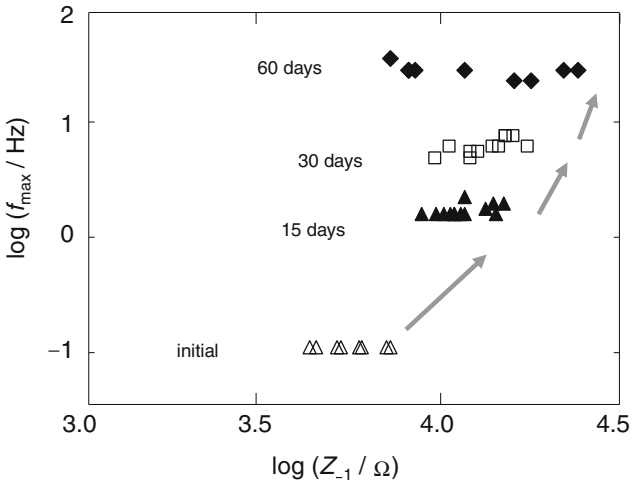

Fig. 11 Variation of the frequency at which this maximum occurs, f_{max}, with logZ_{-1} in replicate EIS experiments for archaeological chain link from the Alcantarins convent (Ontinyent, Valencian Community, Spain) during different stages of its treatment with: 0.05 M Na_2SO_3+0.05 M NaOH (*solid figures*) and 0.10 M NaOH (*empty figures*)

$$\Delta Z_{tot}(t) = \left[\frac{\theta_{corr}(t)}{R_{corr}} + \frac{1-\theta_{corr}(t)}{R_{pas}}\right]^{-1} \quad (1)$$

Then, the fractional surface coverage can be estimated on assuming that, in the initial stage (t=0), all the passive layer is covered by the corrosion layer, so that: $\Delta Z_{tot}(0)=R_{corr}(0)$ and that, at infinite time, the entire piece in contact with the electrolyte is covered by a passive layer ($\Delta Z_{tot}(\infty)=R_{pas}(\infty)$, as:

$$\vartheta_{corr}(t) = \left(\frac{\Delta Z_{tot}(0)}{\Delta Z_{tot}(t)}\right)\left(\frac{\Delta Z_{tot}(t)-\Delta Z_{tot}(\infty)}{\Delta Z_{tot}(0)-\Delta Z_{tot}(\infty)}\right) \quad (2)$$

The above expression, however, neglects the possible variation of the thickness of the corrosion and passive layers with time. To account this factor, one can express the resistance by surface area unit of the corrosion layer and passive layers as:

$$R_{corr}(t) = \frac{\delta_{corr}(t)}{\vartheta_{corr}(t)}\{\chi(t)\rho_{corr} + [1-\chi(t)]\rho_{el}\} \quad (3)$$

$$R_{pas}(t) = \frac{\delta_{pas}(t)}{[1-\vartheta_{corr}(t)]}\rho_{pas} \quad (4)$$

respectively. In the above equations, $\delta_{corr}(t)$, $\delta_{pas}(t)$ represent the thickness of the corrosion and passive layers at time t, $\chi(t)$, the porosity (defined as the volume fraction occupied by the corrosion products) of the corrosion layer [74], and ρ_{el}, ρ_{corr} the resistivities of the electrolyte (filling the pores) and the material(s) forming the corrosion layer, respectively. It is important to note that, as indicated by Turgoose [75], the porosity is taken as a time-dependent variable because placing archaeological iron into an alkaline solution would cause any dissolved Fe^{2+} ions to precipitate within the corrosion layer, decreasing the porosity, restricting the Cl^- ion diffusion, and possibly trapping them [4].

In turn, the capacitance by surface area unit of the corrosion layer, $C_{corr}(t)$, can result, roughly, from the combination of the contributions due to the corrosion materials:

$$C_{corr}(t) = \varepsilon_{corr}\frac{\vartheta_{corr}(t)}{\delta_{corr}(t)}\chi(t) \quad (5)$$

and the electrolyte filling the pores:

$$C_{corr}(t) = \varepsilon_{el}\frac{\vartheta_{corr}(t)}{\delta_{corr}(t)}[1-\chi(t)] \quad (6)$$

ε_{el}, ε_{corr} being the dielectric permittivities of the electrolyte and the corrosion layers, assumed to be time independents. Taking into account that, in contact with aqueous electrolytes, $\varepsilon_{el} \gg \varepsilon_{corr}$, this second contribution can be taken as clearly predominant. Then, combining Eqs. (3)–(6), the frequency $\omega_1(t)$ at a washing time t can be expressed as:

$$\omega_1(t) = (R_{corr}C_{corr})^{-1} = \varepsilon_{el}[1-\chi(t)]\{\rho_{corr}\chi(t) + \rho_{el}[1-\chi(t)]\} \quad (7)$$

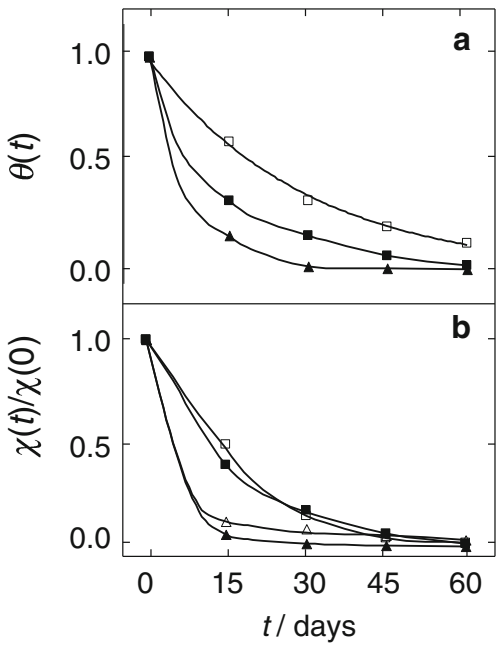

Fig. 12 Variation of *a* $\theta_{corr}(t)$ and *b* $\chi(t)/\chi(0)$, calculated from EIS data, with the time of washing for fragments of nails from the Alcantarins convent (Ontinyent, Valencian Community, Spain) submitted to different stabilization/desalination procedures. *a* 0.10 M NaOH (*squares*), 0.05 M Na_2SO_3+0.05 M NaOH (*solid squares*), and deoxygenated 0.10 M NaOH (*solid triangles*); *b* 0.10 M NaOH (*squares*), deoxygenated 0.10 M NaOH (*solid squares*), and 0.05 M Na_2SO_3+0.05 M NaOH at room temperature (*solid triangles*) and at 50 °C (*triangles*)

Interestingly, the $\theta_{corr}(t)$, $\delta_{corr}(t)$ terms cancel, so that $\omega_1(t)$ can be used to estimate the variations in the porosity of the corrosion layer, $\chi(t)$, during the stabilization/desalination process. For a fast estimate of this variation, Eq. (7) can be simplified on assuming that $\rho_{el} \ll \rho_{corr}$. Accordingly, one can take:

$$C_{corr}(t) \approx \varepsilon_{el}\rho_{corr}\chi(t)[1-\chi(t)] \quad (8)$$

$$C_{corr}(0) \approx \varepsilon_{el}\rho_{corr}\chi(0)[1-\chi(0)] \quad (9)$$

Combining Eqs. (7)–(9) and assuming that the porosities are relatively low ($\chi(t)$, $\chi(0) \ll 1$), yields:

$$\frac{\chi(t)}{\chi(0)} \approx \frac{\omega_1(0)}{\omega_1(t)} \quad (10)$$

Using Eq. (10), it is possible to estimate the variation in the porosity of the corrosion layer from the variation in the frequency of maximum phase angle in the middle-frequency region of the EIS spectra.

Figure 12 a compares the variation of $\theta_{corr}(t)$, calculated from EIS data using Eq. (2), with the time of washing for nails from the Alcantarins convent (Ontinyent, Valencian Community, Spain) submitted to different stabilization/desalination procedures. For treatments in 0.10 M NaOH (squares), 0.05 M Na_2SO_3+0.05 M NaOH (solid squares), and deoxygenated 0.10 M NaOH (solid triangles), $\theta_{corr}(t)$ decreased monotonically with time, experimental curves approaching to an exponential decrease of the corroded area with time. In all cases, the final EIS parameters were coincident, thus denoting that the objects reached a similar stabilized state regardless of the applied desalination treatment. The rate of the exponential decay, however, varied from one to another procedure, the treatment with deoxygenated 0.10 M NaOH being faster than those with 0.10 M NaOH and 0.05 M Na_2SO_3+0.05 M NaOH at room temperature.

Consistently, the time variation of the $\chi(t)/\chi(0)$ ratio calculated from Bode plots using Eq. (10) produced exponential decays. Again, the final state was equivalent, as denoted by the similarity in the EIS data, in particular by the similarity in the maximum phase angle and the frequency at which that phase angle appears, as well as by VMP data, confirming the formation of a magnetite passive layer in the objects after 60 days of treatment. The decay rate was, however, clearly larger for stabilization in 0.05 M Na_2SO_3+0.05 M NaOH baths than for stabilization in NaOH baths. This result would be consistent with the idea that precipitation of dissolved Fe^{2+} ions, resulting from the reduction of Fe(III), in alkaline media, produces a decrease of the porosity of the corroded regions.

The reported methodology provides information for comparing different stabilization procedures applied to archaeological iron. With this regard, however, two aspects should be emphasized: (a) that a more detailed modeling of how the different stabilization/desalination procedures proceed and their influence in the texture, structure, and composition of corrosion and passive layers is needed for properly comparing the effectiveness of such methods and (b) that studies on archaeological iron stabilization must be extended to consider long-term affects where re-corrosion may occur.

Conclusions

EIS measurements on archaeological iron artifacts immersed into air-saturated aqueous $NaClO_4$ solutions can be used to monitor the progress of different stabilization/desalination procedures consisting of watching with 0.10 M NaOH and 0.05 M Na_2SO_3+0.05 M NaOH. A semi-empirical treatment of such data permits to study the variation of the fraction of corroded surface and the porosity of corroded layers relative to its initial porosity with the time of treatment. Both properties decay exponentially with the time of treatment for the studied desalination procedures. The obtained data suggest that all four tested desalination procedures yield to an essentially identical "stable" state, as confirmed by VMP experiments confirming the formation of a passive magnetite layer, but the rate of variation of corroded surface and porosity vary significantly from one procedure to another. Although a more detailed modeling is needed for properly describe the variation in the texture, composition, and structure of corrosion layers of archaeological iron artifacts submitted to stabilizing processes, the reported methodology can aid to perform a systematic evaluation of the effectiveness of such desalination procedures.

Acknowledgments Financial support from the MEC Project CTQ2011-28079-CO3-02 which is supported with ERDF funds is gratefully acknowledged.

References

1. Cronyn JM (1990) The elements of archaeological conservation. Routledge, London
2. Torgoose S (1982) Stud Conservat 27:97–101
3. Keene S, Orton C (1985) Stud Conservat 30:136–142
4. Selwyn L (2004) Overview of archaeological iron: the corrosion problem, key factors affecting treatment, and gaps in current knowledge. Proc. Metal 2004, National Museum of Australia, Canberra, pp 294–306
5. Scott DA, Eggert G (2009) Iron and steel in art: corrosion, colorants, conservation. Archetype, London
6. North NA, Pearson C (1978) Stud Conservat 23:174–186
7. Gilberg MR, Seeley NJ (1982) Stud Conservat 27:180–184
8. Cornell RM, Giovanoli U (1990) Clays Clay Miner 38:469–476
9. Scott DA, Seeley NJ (1987) Stud Conservat 32:73–76
10. Watkinson D (1996) Chloride extraction from archaeological iron: comparative treatment efficiencies. In: Roy A, Smith P (eds)

Archaeological conservation and its consequences. International Institute for Conservation, London, pp 208–212
11. Watkinson D, Al Zahrani A (2008) The Conservator 31:75–86
12. Schmutzler B, Eggert G (2010) Simplifying sodium sulphite solutions—the DBU Project Rettung vom dem Rost. In: Eggert G, Schmutzler B (eds) Archaeological Iron Conservation Colloquium 2010. State Academy of Art and Design, Stuttgart
13. Watkinson D (1982) An assessment of the lithium hydroxide treatments for archaeological ironwork. In: Clarke RW, Blackshaw SM (eds) Conservation of iron, maritime monographs and reports of the National Maritime Museum 53, pp 208–213
14. Wunderlich C-H, Kuhn C, Dröber V, Eggert G, Schleid T (2010) Efficiency of chloride extraction with organic ammonium bases: the Kur-Project "Conservation and Professional Sotrage of Iron Artefacts". In: Eggert G, Schmutzler B (eds) Archaeological Iron Conservation Colloquium 2010. State Academy of Art and Design, Stuttgart
15. Burshneva S, Smirnova N (2010) Some new advances in alkaline sulphite treatment of archaeological iron. In: Eggert G, Schmutzler B (eds) Archaeological Iron Conservation Colloquium 2010. State Academy of Art and Design, Stuttgart
16. de Vivies P, Cook D, Drews MJ, Gonzalez NG, Mardikian P, Memet JB (2007) Transformation of akaganéite in archaeological iron artefacts using subcritical treatment. In: Degrigny C, Van Langh R, Joosten I, Ankersmit B (eds) Proceedings of the International Conference on Metals Conservation, Amsterdam, Netherlands, pp 17–21
17. Mardikian P, Gonzalez N, Drews MJ, Nasanen L (2010) The use of subcritical solutions for the stabilization of archaeological iron artifacts. In: Eggert G, Schmutzler B (eds) Archaeological Iron Conservation Colloquium 2010. State Academy of Art and Design, Stuttgart
18. Dalard F, Gourbeyre Y, Degrigny C (2002) Stud Conserv 47:117–121
19. Adriaens A, Dowsett M, Leyssens K, Van Gasse B (2007) Anal Bioanal Chem 387:861–868
20. Guilminot E, Baron G, Memet JB, Huet N, Le Noc E (2007) Electrolytic treatment of archaeological marine chloride impregnated iron objects by remote control. In: Degrigny C, Van Lang R, Joosten I, Ankersmith B (eds) Metal 07. Proceedings of the Interim meeting of the ICOM-CC Metal WG, vol 3, Amsterdam (the Netherlands). Rijksmuseum Amsterdam, Amsterdam, pp 38–43
21. Liu J, Li Y, Wu M (2008) Stud Conserv 53:41–48
22. Selwyn LS, McKinnon WR, Argyropoulos V (2001) Stud Conservat 46:109–120
23. Schmutzler B, Eggert G (2010) The chloride left behind (dis)solving an analytical problem. In: Eggert G, Schmutzler B (eds) Achaeological Iron Conservation Colloquium 2010. State Academy of Art and Design, Stuttgart
24. Doménech-Carbó A, Lastras M, Rodríguez F, Osete-Cortina L (2013) Microchem J 106:41–50
25. Scholz F, Meyer B (1992) Chem Soc Rev 23:341–347
26. Scholz F, Meyer B (1998) Voltammetry of solid microparticles immobilized on electrode surfaces. In: Bard AJ, Rubinstein I (eds) Electroanalytical Chemistry, A Series of Advances, vol 20. Marcel Dekker, New York, pp 1–86
27. Scholz F, Schröder U, Gulaboski R (2005) Electrochemistry of immobilized particles and droplets. Springer, Berlin
28. Doménech-Carbó A, Doménech-Carbó MT, Costa V (2009) Electrochemical Methods in Archaeometry, Conservation and Restoration. In: Scholz F (ed) Monographs in electrochemistry series. Springer, Berlin
29. Doménech-Carbó A (2010) J Solid State Electrochem 14:363–379
30. Doménech-Carbó A (2012) Electrochemical techniques. In: Edwards HGM, Vandenabeele P (eds) Analytical Archaeometry, selected topics, chapter 7. The Royal Society of Chemistry, London
31. Doménech-Carbó A, Labuda J, Scholz F (2013) Pure Appl Chem 85: 609–631
32. Doménech-Carbó A (2011) Anal Methods 3:2181–2188
33. Doménech-Carbó A (2012) Electrochemical analysis: voltammetry of microparticles. In: Dillmann P, Adriaens A, Angelini E, Watkinson D (eds) Corrosion and conservation of cultural heritage metallic artefacts (Chapter II.7). European Federation of Corrosion, Maney, Leeds
34. Walter GW (1981) J Electroanal Chem 118:259–273
35. Murray JN (1997) Progr Org Coat 31:375–391
36. Bastidas JM, Polo JL, Cano E, Torres CL, Mora N (2000) Mater Corros 51:712–718
37. Bastidas JM, Polo JL, Torres CL, Cano E (2001) Corros Sci 43:269–281
38. Alves VA, Brett CMA (2002) Electrochim Acta 47:2081–2091
39. Polo JL, Cano E, Bastidas JM (2002) J Electroanal Chem 537:183–187
40. Park JJ, Pyun SI (2003) J Solid State Electrochem 7:380–388
41. Evesque M, Keddam M, Takenouti H (2004) Electrochim Acta 49: 2937–2943
42. Li WS, Cai SQ, Luo JL (2004) J Electrochem Soc 151:B220–B226
43. Mora N, Cano E, Polo JL, Puente JM, Bastidas JM (2004) Corros Sci 46:563–568
44. Chiavari C, Colledan A, Frignani A, Brunoro G (2006) Mater Chem Phys 95:252–259
45. Chiavari C, Rahmouni K, Takenouti H, Joiret S, Vermaut P (2007) Electrochim Acta 52:7760–7769
46. Liu W, Zhang H, Qu Z, Zhang Y, Li J (2010) J Solid State Electrochem 14:965–973
47. Toledo-Martos LA, Pech-Canul MA (2011) J Solid State Electrochem 15:1927–1934
48. Cano E, Lafuente D, Bastidas DM (2010) J Solid State Electrochem 14:381–391
49. Grassini S, Angelini E, Parvis M, Bouchar M, Dillmann P, Neff D (2013) Appl Phys A. doi:10.1007/s00339-013-7724-1
50. Hernandez-Escampa M, Gonzalez J, Uruchurtu-Chavarin J (2010) J Appl Electrochem 40:345–356
51. Young L (1961) Anodic oxide films. Academic, New York
52. Rosas-Camacho O, Urquidi-Macdonald M, Macdonald DD (2009) ECS Trans 19:143–165
53. Macdonald DD, Engelhardt GL (2010) ECS Trans 28:123–144
54. Sharifi-Asl F, Taylor ML, Lu Z, Engelhardt GL, Kursten B, Macdonald DD (2013) Electrochim Acta 102:161–173
55. Macdonald DD (2011) Electrochim Acta 56:1761–1772
56. Macdonald DD, Sikora A, Engelhardt G (1998) Electrochim Acta 43: 87–107
57. Grygar T (1996) J Electroanal Chem 405:117–125
58. Grygar T (1997) J Solid State Electrochem 1:77–82
59. Xu J, Huang W, McCreery RL (1996) J Electroanal Chem 410:235–242
60. Kuang F, Zhang D, Li Y, Wan Y, Hou B (2009) J Solid State Electrochem 13:385–390
61. Chen G, Waraksa CC, Cho H, Macdonald DD, Mallouk TE (2003) J Electrochm Soc 150:E423–E428
62. Rimmer M, Watkinson D, Wang Q (2012) Stud Conservat 57:29–41
63. Poljacek SM, Risovic D, Cigula T, Gojo M (2012) J Solid State Electrochem 16:1077–1089
64. Sluythers-Rehnach M (1994) Pure Appl Chem 66:1831–1891
65. Boukamp BA, Bouwmeester HJM (2003) Solid State Ionics 157:29–33
66. Ibrahim MAM, Pongkao D, Yoshimura M (2002) J Solid State Electrochem 2002(6):341–350
67. Xia Z, Nanjo H, Aizawa T, Kanakubo M, Fujimura M, Onagawa J (2007) Surf Sci 601:5133–5141

68. Lee S-J, Pyun S-I (2007) J Solid State Electrochem 11:829–839
69. Raistrick ID (1990) Electrochim Acta 35:1579–1586
70. Doménech-Carbó A, Doménech-Carbó MT, Peiró MA (2011) Electroanalysis 23:1391–1400
71. Doménech-Carbó A, Doménech-Carbó MT, Pasíes T, Bouzas MC (2012) Electroanalysis 24:1945–1955
72. Mutombo P, Hackerman N (1997) J Solid State Electrochem 1:194–198
73. Fetisov VB, Ermakov AN, Belysheva GM, Fetisov AV, Kamyshov VM, Brainina KZ (2004) J Solid State Electrochem 8:565–571
74. Venkatram MS, Cole IS, Emmanuel B (2011) Electrochim Acta 56: 8192–8203
75. Turgoose S (1993) Structure, composition and deterioration of unearthed iron objects. In: Current problems in the conservation of metal antiquities. Tokyo National Research Institute of Cultural Properties, Tokyo, pp 35–52